ACS APPLIED POLYMER MATERIALS

pubs.acs.org/acsapm
Article

Role of Polymer Architecture in CO_2 Capture from Air Using Supported Poly(alkylenimine)s: Linear vs Branched Polymers

Jacob Hoffman, Laura Proaño, and Christopher W. Jones*

Cite This: ACS Appl. Polym. Mater. 2025, 7, 15671−15681
Read Online

ACCESS | Metrics & More | Article Recommendations | Supporting Information

ABSTRACT: Direct air capture (DAC) of CO_2 coupled with geologic storage is a promising climate change mitigation strategy, with some applications employing amines supported on porous solids as CO_2 sorbents. While branched poly(ethylenimine) (PEI) is the standard benchmark amine material, it suffers from limited oxidative stability. Poly(propylenimine) (PPI), as an alternative, has previously demonstrated improved resistance to degradation under harsh oxidative conditions. Linear and branched PEI are commercially available, though at different molecular weights, while PPI is not commercially available. For this reason, a comparative study of all four polymers (linear PEI, branched PEI, linear PPI, branched PPI) has not been reported for DAC. In this study, we synthesize and compare low-molecular-weight (~800 g/mol) linear (L) and branched (B) PEI and PPI supported on a model support, SBA-15 silica. These materials are evaluated for CO_2 adsorption under dry, DAC-relevant conditions (400 ppm of CO_2, 30 °C). LPPI exhibited the highest amine efficiency at all loadings, reaching a maximum of 0.14 mmol CO_2/mmol N, outperforming BPEI, while LPEI consistently showed the lowest uptake capacity. Temperature-programmed desorption reveals that the structure of the amine polymer impacts the CO_2 binding strength, with branched polymers displaying higher desorption energies of 102−111 kJ/mol. *In situ* infrared spectroscopy experiments show that all sorbents preferentially capture CO_2 as ammonium carbamate. Isobaric CO_2 uptake studies further underscore the influence of polymer mobility and support pore crowding on performance, while demonstrating the sorbents' performance at elevated temperatures and CO_2 concentrations. All materials demonstrated good stability over 25 adsorption−desorption cycles using thermal regeneration in an inert gas purge, with only BPPI displaying a 10−11% decrease in capacity/amine efficiency during cycling, possibly due to the loss of low molecular weight, oligomeric amines. This is the first side-by-side comparison of the CO_2 sorption properties of linear and branched PEI and PPI with similar molecular weights. These findings highlight the significant role of polymer architecture in CO_2 capture efficiency and inform future designs of durable, high-performance DAC sorbents.

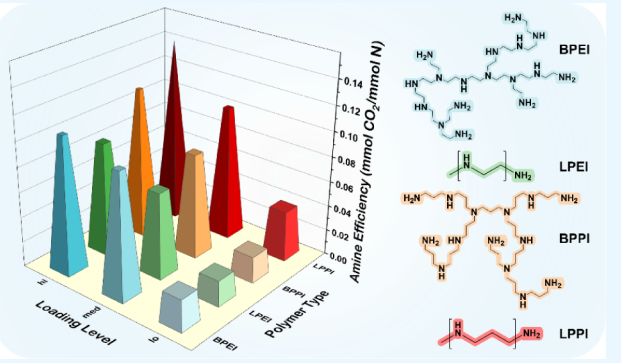

KEYWORDS: *direct air capture, adsorbents, stability, amine efficiency, cyclic capacity, desorption energy*

INTRODUCTION

The increasing concentration of carbon dioxide (CO_2) in the atmosphere since rapid industrialization and the initial usage of fossil fuels in the 19th century is widely regarded as the primary cause of climate change.[1] The speedy and widespread rollout of carbon-neutral energy sources, combined with the retirement of carbon-intensive ones, is and will continue to be the most significant measure to combat rising greenhouse gas levels.[2] However, atmospheric carbon removal technologies are gaining traction as the largest countries fall behind their emissions targets. Among these, the removal of carbon dioxide from the atmosphere by chemical means, also referred to as direct air capture (DAC) of CO_2, is one of the most scalable.[3−5] When combined with geologic sequestration on a large scale, DAC can provide a way to reduce the atmospheric CO_2 concentration.[6]

The most well-studied mode of DAC is temperature swing adsorption or temperature-vacuum swing adsorption. Solid amine adsorbents are among the most effective DAC adsorbents, offering excellent CO_2 capacities and selectivities to CO_2 over N_2 and O_2.[7,8] The prototypical DAC sorbent uses low molecular weight (~800 Da), branched poly(ethylenimine) (BPEI) supported on a porous support such as silica, alumina, zeolites, MOFs or COFs.[9−16] BPEI is highly effective and its high primary and secondary amine density, existence as a viscous liquid with low volatility, and its

Received: September 14, 2025
Revised: November 10, 2025
Accepted: November 11, 2025
Published: November 17, 2025

commercial availability make it a popular ingredient in DAC sorbents. However, it suffers from low stability in oxidative environments, and this limits its useful lifetime, leading to high sorbent replacement costs, currently limiting its large-scale use.[17−23]

For these reasons, the development of alternative supported amines based on impregnated polymers or grafted aminosilanes has been a focus of research for over a decade.[16,24−26] Among the oligomeric or polymeric amines, both main chain aminopolymers such as poly(propylenimine) and side chain aminopolymers such as poly(allylamine) and poly(glycidylamine) have been developed.[27−30] In a prior study, small, molecular analogues of poly(ethylenimine) and poly(propylenimine) were supported on a porous silica support and evaluated for CO_2 capture under simulated DAC conditions.[31] The propylenimine structures offered competitive CO_2 sorption capacities and enhanced stability toward oxidation compared to the ethylenimine analogues.[31,32] Subsequent studies of linear poly(propylenimine) (LPPI) and branched poly(propylenimine) (BPPI) at several molecular weights demonstrated these polymers to be potential alternatives to the BPEI materials used ubiquitously around the world as an amine DAC benchmark material.[33−35] However, both LPPI and BPPI are not widely commercially available. Furthermore, the linear poly(ethylenimine) analogue, LPEI, while commercially available, is only available at higher molecular weights, with the lowest molecular weight commonly offered 2500 DA. This makes direct comparisons to commercial BPEI challenging.[36−39]

In this work, we prepare LPEI, LPPI and BPPI in the laboratory at a common molecular weight to enable a direct, side-by-side comparison of the effectiveness of these different amine polymers to commercial BPEI under simulated, dry DAC conditions. Because the benchmark BPEI is ∼ 800 DA molecular weight, oligomeric LPEI, LPPI and BPPI were made at similar molecular weights, characterized, and then impregnated into a mesoporous silica SBA-15 model support material. The results demonstrate that LPPI slightly outperforms BPEI regarding dry CO_2 capacity at 400 ppm of CO_2 conditions, though all of the amine polymers offer useful CO_2 sorption performance at 30 °C. To our knowledge, this is the first side-by-side comparison of these four polymers at comparable conditions, on a common support, for DAC.

EXPERIMENTAL SECTION

Materials. Methanol, hydrobromic acid (48%), ethylenediamine, 1,3 diaminopropane, 2-ethyl-2-oxazoline, triethylamine, Ambersep 900(OH), Pluronic *p*-123 block copolymer and tetraethyl orthosilicate were acquired from Sigma-Aldrich. 3-amino-1-propanol and anhydrous zinc chloride were acquired from Alfa Aesar. Anhydrous acetonitrile, calcium hydride and azetidine (98%) were acquired from Thermo Scientific. Methyl-*p*-toluenesulfonate was acquired from TCI America. Ammonium hydroxide was acquired from Fisher Scientific. Hydrochloric acid (37%) was acquired from VWR. All gases were sourced from Airgas.

METHODS

Synthesis of SBA-15. The synthesis procedure for SBA-15 followed previously published methods.[33] In a typical synthesis, 27.6 g of Pluronic *p*-123 coblock polymer was added to a 2 L conical flask. Next, 732 g of deionized water was added, followed by 130 mL of 37% hydrochloric acid and the contents were stirred for 3 h at room temperature until solids were fully dissolved. Then, 50.1 g of tetraethyl orthosilicate was added dropwise and the contents stirred for 20 h at 40 °C. The flask was capped, insulated and kept undisturbed in an oil bath at 120 °C for 24 h. The mixture was cooled and 450 mL of deionized water was added to quench the reaction. The precipitate was washed with deionized water during vacuum filtration several times until the filtrate was clear. The precipitate was transferred to a ceramic dish and dried for 12 h at 75 °C. The solid was then calcined using the following procedure: ramp to 200 °C at 1.2 °C per min; hold for 1 h; ramp to 550 °C at 1.2 °C per min; hold for 12 h; cool to room temperature. The powder was finally collected and stored under ambient conditions.

Linear Poly(propylenimine) Synthesis. The synthesis of linear poly(propylenimine) was adapted from Pang et al.[33] Anhydrous acetonitrile (115 mL, 2.2 mol) was added to a 500 mL round-bottom flask along with a stir bar. $ZnCl_2$ (5.5 g, 0.04 mol) was added all at once and dispersed. 3-amino-1-propanol (150.2 g, 2 mol) was added dropwise while stirring. The flask was heated to 95 °C and held for 48 h under refluxing. The mixture was cooled to room temperature and excess acetonitrile was removed by rotary evaporation at 30 °C. The mixture was vacuum distilled to isolate the 6-member ring monomer 2-methyl-5,6-dihydro-4H-1,3-oxazine (MeOZI).

MeOZI and acetonitrile were dried by stirring each individually with calcium hydride overnight. They were collected by vacuum distillation in respective Strauss flasks, which were backfilled with argon until proceeding in subsequent steps. Dried MeOZI (10.3 g, 0.1 mol) was added via needle to a torch-dried and argon-purged Schlenk tube capped with a rubber septum and with a stir bar inside. Dried acetonitrile (52 mL, 1 mol) was added via needle and the mixture was stirred briefly. With a strong argon flow applied through the neck of the tube, methyl-p-toluenesulfonate (2.16 g, 0.0116 mol) was added by briefly removing the septum. The mixture was purged by bubbling argon for 1 h. It was then submerged in an oil bath and left stirring for 48 h at 90 °C. 1,3-diaminopropane (1.95 mL, 0.025 mol) was added via needle and the reaction was cooled to room temperature. Acetonitrile and 1,3-diaminopropane were removed by rotary evaporation at 50 °C.

Hydrolysis of the side chain was performed by stirring with 5 M HCl (200 mL) for 48 h at 100 °C under reflux. The flask was cooled, and acetic acid was removed via rotary evaporation at 50 °C. The resulting slurry was stirred in an ice bath, 10 M NaOH was added dropwise to adjust the pH to 13 and then centrifuged. The precipitate was washed twice with NH_4OH (14.8M), once with a 1:4 mixture of triethylamine in DI water and once with only DI water, centrifuged after each wash. The final precipitate was dissolved in methanol, filtered and dried via rotary evaporation and high vacuum (<20 mTorr). ^1H NMR (500 MHz, CD_3OD) was performed to ascertain the molecular weight of the polymer (Figure S6).

Linear Poly(ethylenimine) Synthesis. The synthesis of linear PEI was adapted from previously detailed procedures.[33,40] Anhydrous acetonitrile and 2-ethyl-2-oxazoline were dried by stirring each individually with calcium hydride overnight. The two were isolated by vacuum distillation, collecting each in respective Strauss flasks, which were backfilled with argon until the next step. Dried 2-ethyl-2-oxazoline (8.14 g, 0.08 mol) was added via needle to a torch-dried and argon-purged Schlenk tube capped with a rubber septum with a stir bar inside. Dried acetonitrile (62 mL, 1.19 mol) was added via needle and the mixture was stirred briefly. With a strong argon flow applied through the neck of the tube, methyl-p-toluenesulfonate (1.28 g, 0.0067 mol) was added by briefly removing the septum. The mixture was purged by bubbling argon for 1 h. It was then submerged in an oil bath and left stirring for 48 h at 80 °C. Ethylenediamine (0.9 mL, 0.014 mol) was added via needle and the reaction was cooled to room temperature. Acetonitrile and ethylenediamine were removed by rotary evaporation at 50 °C.

Hydrolysis of the side chain was performed by stirring with 5 M HCl (162 mL) for 48 h at 110 °C under reflux. The flask was cooled and propanoic acid was removed via rotary evaporation at 50 °C. The resulting slurry was stirred in an ice bath, 10 M NaOH was added dropwise to adjust the pH to 13 and then centrifuged. The precipitate was washed twice with NH_4OH (14.8M) and once with DI water, centrifuged after each wash. The final precipitate was dissolved in

https://doi.org/10.1021/acsapm.5c03465
ACS Appl. Polym. Mater. 2025, 7, 15671−15681

methanol, filtered and dried via rotary evaporation and high vacuum (<20 mTorr). ^{1}H NMR (500 MHz, CD_3OD) was performed to attain the molecular weight of the polymer (Figure S7).

Branched Poly(propylenimine) Synthesis. The synthesis of branched PPI was adapted from the method developed by Sarazen et al.[34,35] Methanol (20 mL, 0.49 mol) and azetidine (98%, 1.31 mL, 0.02 mol) were added to a pressure flask with a stir bar. HBr (48%, 540 μL) was added and the flask sealed. The reaction was stirred at 90 °C for 88 h then cooled to room temperature. Methanol was removed by rotary evaporation at 30 °C. The result was solubilized in 50 mL of DI water, to which 70 g of AmberSep 900(OH) resin was added and stirred very slowly (50 rpm) for 48 h. The mixture was filtered and the liquid dried by rotary evaporation. A second resin treatment was performed by the same process with 30 mL of DI water and 50 g of resin. After drying, the polymer was solubilized in methanol, passed through a syringe filter (0.22 μm PTFE) and dried by rotary evaporation and high vacuum (<20 mTorr). ^{1}H NMR (500 MHz, D_2O) was performed. Matrix-assisted laser desorption/ionization (MALDI) mass spectrometry was performed to attain the molecular weight of the polymer (Figure S5).

Composite Preparation. Composites of polymer and SBA-15 were prepared via a wet impregnation method. The desired amount of polymer was dissolved in 5 mL of methanol. Meanwhile, the desired amount of SBA-15 and 15 mL of methanol were added to a 100 mL round-bottom flask and left to stir for at least 1 h to uniformly disperse. The polymer solution was transferred to the support suspension and left to stir overnight. The methanol was removed by rotary evaporation at 50 °C then dried overnight at room temperature under high vacuum (<20 mTorr). The dried composites were collected and stored under argon in wrapped glass vials.

Organic Combustion to Assess Polymer Loading. Organic combustion experiments were performed using a TA Instruments TGA 550 to measure the organic content of the sorbents (Figure S4). Samples were held at 110 °C under a nitrogen purge for 1 h to desorb water and other adsorbed species. The purge gas was switched to air and the temperature was ramped 10 °C/min to 700 °C and held there for an additional 30 min. The mass loss between 110 °C and the end of the experiment was normalized by the residual mass to obtain the organic content.

Nitrogen Physisorption. Micromeritics Tristar II Plus was used to perform nitrogen physisorption at 77 K. Samples were dried at 60 °C on a vacuum line reading 30 Torr for 12 h. Surface area was estimated by applying BET theory between P/P_0 0.05−0.2. Total pore volume was determined using the amount adsorbed at P/P_0 of 0.95. Pore filling was calculated by the difference in total pore volume normalized by the pore volume of the blank support.

CO_2 Adsorption. The pseudoequilibrium CO_2 sorption capacities of the sorbent were determined using a TA Instruments TGA 550. The powdered sorbents (~10 mg) were held at 110 °C for 3 h under a nitrogen stream. The temperature was ramped down to the adsorption temperature of 30 °C, the inlet gas switched to 400 ppm of CO_2 in nitrogen and held for 12 h. The samples were desorbed by ramping to and holding for 1 h at 110 °C under nitrogen.

Temperature-Programmed Desorption. Temperature-programmed desorption was performed following 12 h of adsorption under 400 ppm of CO_2 at 30 °C in a TGA. The samples (~10 mg) were held for 1 h under a nitrogen purge at the adsorption temperature. The temperature was then ramped to 110 °C at 0.5 °C/min and held at 110 °C for 1 h. The experiment was repeated with fresh samples using ramp rates of 0.3 and 1.0 °C/min. A LiCOR 850 CO_2/H_2O analyzer was utilized to monitor the CO_2 concentration of the outlet through the entire process.

CO_2 Isobars. CO_2 isobars were measured using a TA Instruments TGA Q500. Samples (~8 mg) were activated for 390 min at 110 °C under N_2, after which they were cooled and equilibrated at 30 °C. The gas flow was switched to 400 ppm or 10% CO_2 in N_2 for 390 min. The temperature was then raised at 10 °C/min to 40 °C and held for 390 min. This was repeated in 10 °C increments up to 90 °C and then reversed back down to 30 °C, holding for 390 min at each temperature.

Thermal Sorption−Desorption Cycling. A TA Instruments Q500 TGA was used. Samples (~8 mg) were kept at 110 °C for 3 h under a nitrogen stream. The temperature was lowered at 10 °C/min to 30 °C and the flow switched to 400 ppm of CO_2/N_2 for 1 h of adsorption. The flow was then reverted to nitrogen and the temperature ramped at 10 °C/min to 110 °C, stabilized and kept for 10 min for desorption. This adsorption−desorption cycling was repeated 24 more times.

Diffuse Reflectance Infrared Fourier Transform Spectroscopy. *In situ* FT-IR spectroscopy was performed on an Invenio Bruker IR spectrometer with a low-temperature diffuse reflectance infrared Fourier transform spectroscopy (DRIFTS) cell (CHC−CHA-4, Harrick Scientific Products Inc.). The sample holder inside the DRIFTS cell chamber was filled with about 15−20 mg of sample. The sample was activated at 100 °C under 70 mL/min Ar flow for 1 h. The temperature was cooled to 30 °C and the inlet gas flow was switched to dry 400 ppm of CO_2/N_2 (70 mL/min). During the adsorption, 400 spectra were collected with 60 scans at a resolution of 4 cm^{-1} every 30 s for a total period of ~ 200 min.

RESULTS AND DISCUSSION

Sorbent Characteristics. Linear poly(ethylenimine) ($M_n \approx 740$ g/mol), linear poly(propylenimine) ($M_n \approx 760$ g/mol) and branched poly(propylenimine) ($M_n \approx 740$ g/mol) were synthesized according to the methods described in the Experimental Section. Physically impregnated composites of aminopolymers in SBA-15 were prepared by a wet impregnation method, targeting low (4.4 ± 0.5 mmol N/g SBA-15), medium (10.7 ± 1.3 mmol N/g SBA-15) and high (17.8 ± 1.9 mmol N/g SBA-15) amine loadings. Organic and amine loadings were verified by combustion TGA and the BET surface areas and pore volumes were obtained from cryogenic N_2 physisorption data (Table 1). As expected, surface area and pore volume decreased with increasing polymer loading due to the deposition of amine polymer within the pores. Of all the composite types, LPEI-impregnated SBA-15 appeared to retain

Table 1. Physical Characteristics of Aminopolymer-Impregnated SBA-15 Sorbents

	Organic loading [wt %]	Amine loading [mmol N/g SBA-15]	B.E.T. Surface Area [m^2/g]	Pore volume [cm^3/g]	Pore fill [%]
SBA-15	---	---	790	0.93	---
BPEI low	17	4.9	407	0.65	30
BPEI med	36	13.0	148	0.26	72
BPEI high	46	19.5	44	0.08	91
LPEI low	15	4.1	467	0.72	23
LPEI med	29	9.8	288	0.49	48
LPEI high	42	17.1	179	0.30	68
BPPI low	18	3.9	374	0.59	36
BPPI med	37	10.3	143	0.26	73
BPPI high	48	15.9	31	0.05	95
LPPI low	21	4.9	424	0.69	27
LPPI med	35	9.6	211	0.37	60
LPPI high	51	18.7	12	0.03	97

https://doi.org/10.1021/acsapm.5c03465
ACS Appl. Polym. Mater. 2025, 7, 15671−15681

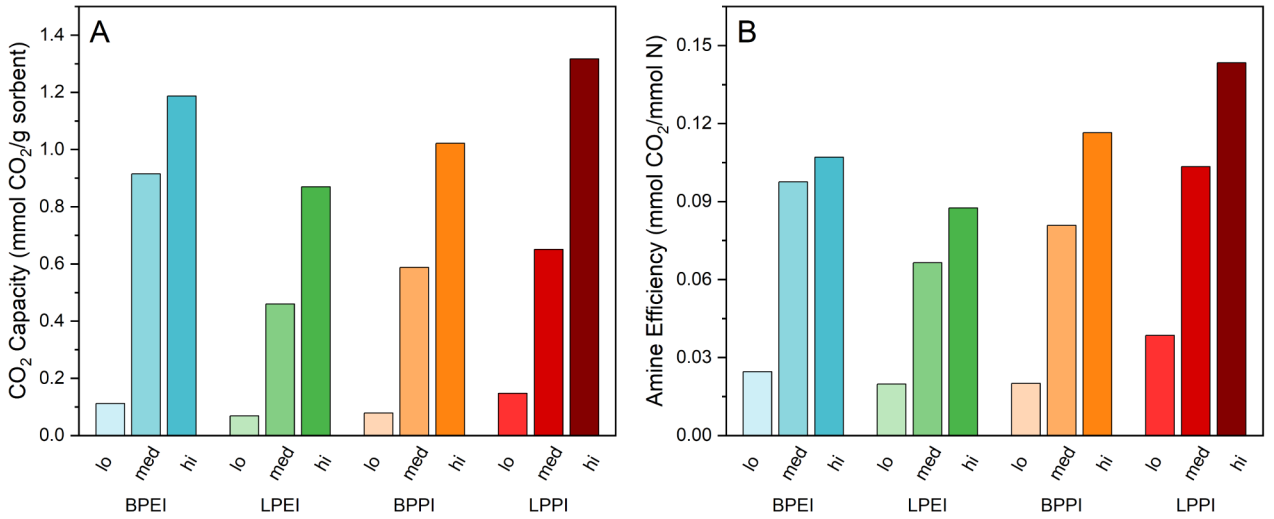

Figure 1. (A) CO_2 capacity and (B) amine efficiencies of all four polymers in SBA-15 at each loading level. Adsorption performed at 30 °C and 400 ppm of CO_2/N_2 balance for 12 h following 3 h activation at 110 °C.

significantly more of its pore volume, with only 68% of pore volume occupied even at the highest polymer loading. Compared to the others, which all show 90−100% of their pore volume occupied at the highest amine loading, this is remarkably low and suggests that the packing of LPEI is particularly effective, as revealed by previous studies, and/or more LPEI deposits on the silica's external surface.[41−43] Meanwhile, BPPI appears to occupy more space within the pores than the others at all loading levels on a per amine basis, likely a result of its branched architecture and the additional $-CH_2-$ in its structure compared to PEI (Table S2).

CO_2 Adsorption. CO_2 capacities were measured using 400 ppm of CO_2 in nitrogen to attain the capacity of the four sorbent types at all amine loadings (Figure 1). The sorbents were activated at 110 °C for 3 h, followed by adsorption at 30 °C for 12 h. All materials display an increase in capacity with higher amine loading, as expected. Linear PEI displays the lowest capacity and amine efficiency at all polymer loadings. Linear PEI-based sorbents have previously been observed to underperform compared to BPEI when exposed to pure CO_2, which was attributed to LPEI having a lower mobility within the support pores.[44] Linear PEI is a semicrystalline solid and branched PEI is viscous liquid in the bulk; it has been suggested that that remains true within the pores, accounting for the difference.[44] Additionally, branching within BPEI affords it several primary amine sites per molecule, whereas LPEI, as synthesized, only has primary amines at the chain ends, the rest being secondary amines. Primary amines have been previously shown to be more effective at capturing CO_2, particularly at ultradilute concentration, leading to the superior performance of BPEI.[45,46]

In terms of capacity, the BPPI-impregnated SBA-15 samples displayed lower uptake than the corresponding BPEI composites across all loading levels. On a weight basis, as with CO_2 capacity, BPPI modestly underperforms BPEI due to the additional carbon in the polymer chains. On an amine basis, though, its performance is closer to that of BPEI, which could be due to the larger intramolecular distance between amine sites. The cooperation of two amine sites is crucial to the formation of alkylammonium carbamate, the adsorbed form of CO_2, and the increased distance between these sites due to the propyl spacer can isolate them such that this coordination is more difficult. Only at the highest organic loading does BPPI have a slightly higher amine efficiency than BPEI (0.12 vs 0.11 mmol CO_2/mmol N, respectively) which could be due to the higher amine density of BPEI or a higher degree of intermolecular amine coordination that only becomes a factor with overcrowding of the pores.

While BPEI has the highest capacity (0.91 mmol/g) of all the medium loading samples, LPPI overtakes it in terms of amine efficiency due to the higher amine density of PEI compared to PPI. In fact, linear PPI sorbents display the highest amine efficiency at all loading levels (Table S1). This could be due to the increased basicity of amine sites between propyl spacers compared to those separated by ethyl spacers.[47] Additionally, linear PPI in the bulk is a partially crystalline solid powder, whereas branched PEI is a viscous liquid (Figure S9). This suggests that linear PPI chains are capable of cross chain coordination that aligns amine groups, thereby promoting ammonium carbamate formation. This might imply that linear PEI, which is also a solid in the bulk, should benefit from the same arrangement, though the results here show it has the worst performance. However, the fractional pore fillings for the linear PEI samples are the lowest of all materials (Table 1). The highest loaded LPEI sorbent has a pore filling of only 68%, on par with the medium loading of the other three composites. This would suggest that cross-chain coordination and hydrogen bonding is so effective that LPEI forms a tightly packed polymer layer along the pore walls and the CO_2 may struggle to penetrate it at the low DAC CO_2 concentration, or that there is excessive LPEI deposited on the silica external surface, with that dense film also making some amine sites inaccessible. However, XPS results suggest that the surface of LPEI-impregnated SBA-15 did not have a disproportionate concentration of polymer, probed via the nitrogen concentration, compared to the general polymer concentration of the samples, as measured by combustion TGA (Table S3).

CO_2 Desorption. Temperature-programmed desorption (TPD) was performed to study the binding strength of CO_2 on the materials following 12 h of adsorption using 400 ppm of CO_2. Initially, the temperature was held at 30 °C for 1 h under a nitrogen stream to purge physisorbed species,[48] and then the temperature was ramped at 0.5 °C/min to 110 °C while

https://doi.org/10.1021/acsapm.5c03465
ACS Appl. Polym. Mater. 2025, 7, 15671−15681

monitoring the outlet CO_2 concentration. The temperature at which the concentration peaked is referred to as T_{peak} and is labeled for each amine species in Figure 2A. The location of

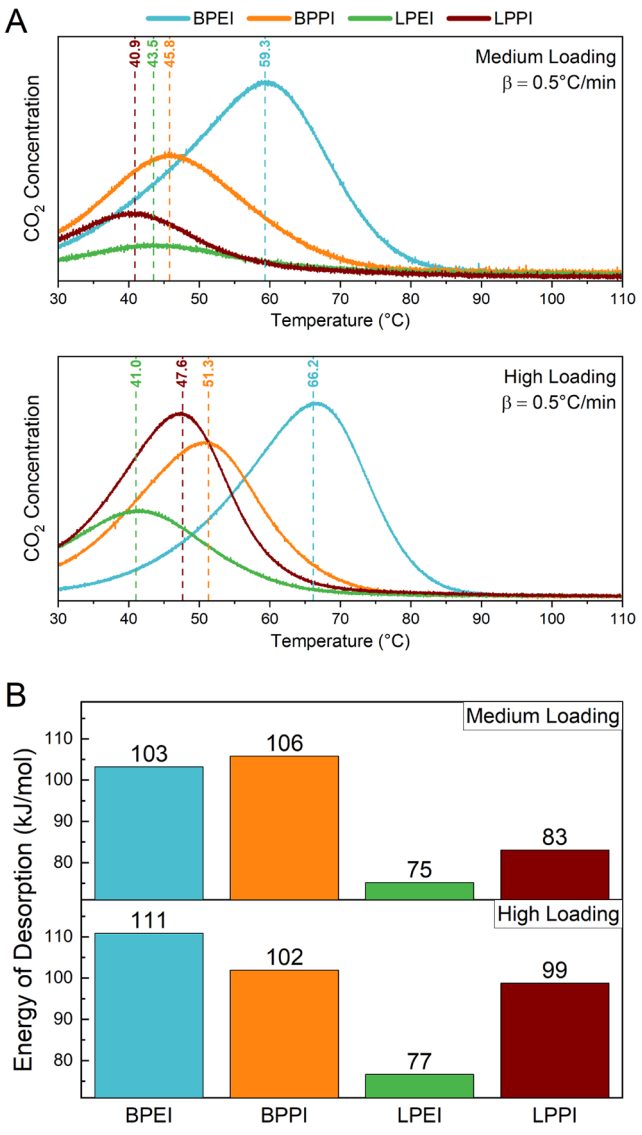

Figure 2. A) CO_2 TPD profiles and B) energy of CO_2 desorption of medium and high loaded aminopolymer/SBA-15 composites following 12 h of adsorption under 400 ppm of CO_2 at 30 °C. Energy of desorption (E_d) was obtained by following the method detailed by Cvetanovic et al.[52] β: temperature ramp rate during TPD.

this peak is indicative of a combination of the strength of the chemisorption and the polymer properties, such as polymer chain mobility. Other factors, like support pore and particle size, can be removed from consideration, since the same parent support batch was used in all materials.

The desorption profiles show that the branched polymer species display higher T_{peak} values than those of the linear species, with BPEI having a significantly higher T_{peak}. This can be due in part to the preferred formation of ammonium carbamate, a stronger chemisorption product than carbamic acid, on his material, though IR data discussed below do not support this as the cause.[49] As noted above, polymer mobility likely also plays a role, in that CO_2 will be able to more effectively penetrate into polymer layers and agglomerates if a polymer is more mobile, thereby requiring more energy and higher temperature to expel CO_2 from the depths of the polymer during desorption. One previous study has demonstrated that a branched PEI based sorbent had higher energies of activation for CO_2 desorption than a linear PEI sorbent, which was attributed to the energy input required to first straighten the polymer chains of BPEI before CO_2 can be released.[50] Additionally, a study featuring TPD following humid CO_2 capture suggests that the delayed desorption of CO_2 when water was present during adsorption is due to the water-enhanced penetration of CO_2 into the intrapore polymer film.[51] Thus, during desorption, the elongated diffusion path for CO_2 out of the film leads to delayed desorption peaks in the TPD profile. Similarly, in comparing the four polymer types in this current work, the higher desorption temperature of BPEI- and BPPI-impregnated SBA-15 may indicate that CO_2 is more effective at penetrating these intraparticle polymer domains as compared to the linear species, with BPEI having the most accessible polymer nanodomains.

By repeating the TPD experiment using two additional ramp rates, we can calculate the apparent energy of CO_2 desorption (E_d).[52] Figure 2B displays the energy of desorption for the four aminopolymer-impregnated SBA-15 composites at medium and high amine loadings. As noted above for the peak desorption temperatures, the higher energies of desorption for the branched species could indicate stronger bond formation due to the preferred formation of ammonium carbamate over carbamic acid (see below) and/or more effective polymer penetration and retention of CO_2 during adsorption and desorption, respectively. Interestingly, the LPPI-impregnated SBA-15 shows a considerable increase in E_d from 83 to 99 kJ/mol when switching from medium to high polymer loading. Previous studies comparing linear and branched PEI-impregnated silica showed similar trends, with lower CO_2 desorption temperatures and activation energies for LPEI than BPEI across all adsorption conditions.[36,50] Additionally, they found that a higher polymer loading within the support correlates with a higher T_{peak} and E_d due to a higher diffusive barrier for CO_2 desorption.

***In Situ* DRIFTS.** To further understand the CO_2 reaction mechanisms at play inside the pores, *in situ* FTIR was performed in the presence of flowing 400 ppm of CO_2 over the course of 3 h. Figure 3 shows the time evolution of the adsorbed species. While all four spectra display certain distinct bands that are common across the samples, there are some points of interest. The spectra of BPEI and BPPI show a resemblance to one another, particularly in the prominence of peaks around 1620−1630 cm^{-1} ($\delta_{as}NH_3^+$) and 1487−1512 cm^{-1} (νCOO^-), previously attributed to ammonium ion and carbamate ion formation, respectively (see Table 2 for peak assignment sources). LPPI displays a shoulder around 1620 cm^{-1} ($\delta_{as}NH_3^+$), but LPEI largely lacks intensity at this frequency. BPPI and LPPI both display particularly sharp peaks at 1410−1420 cm^{-1}, associated with carbamate C−N stretching and/or skeletal vibrations.

Notably, none of the spectra display peaks in the 1650−1700 cm^{-1} range that have historically been attributed to the formation of carbamic acid.[53−55] Thus, there is no support for the hypothesis that the lower desorption temperature and energy requirement observed for the linear polymers here compared to the branched polymers is associated with the formation of carbamic acid instead of carbamate. This, in addition to the fact that the TPD curves (Figure S2) display

https://doi.org/10.1021/acsapm.5c03465
ACS Appl. Polym. Mater. 2025, 7, 15671−15681

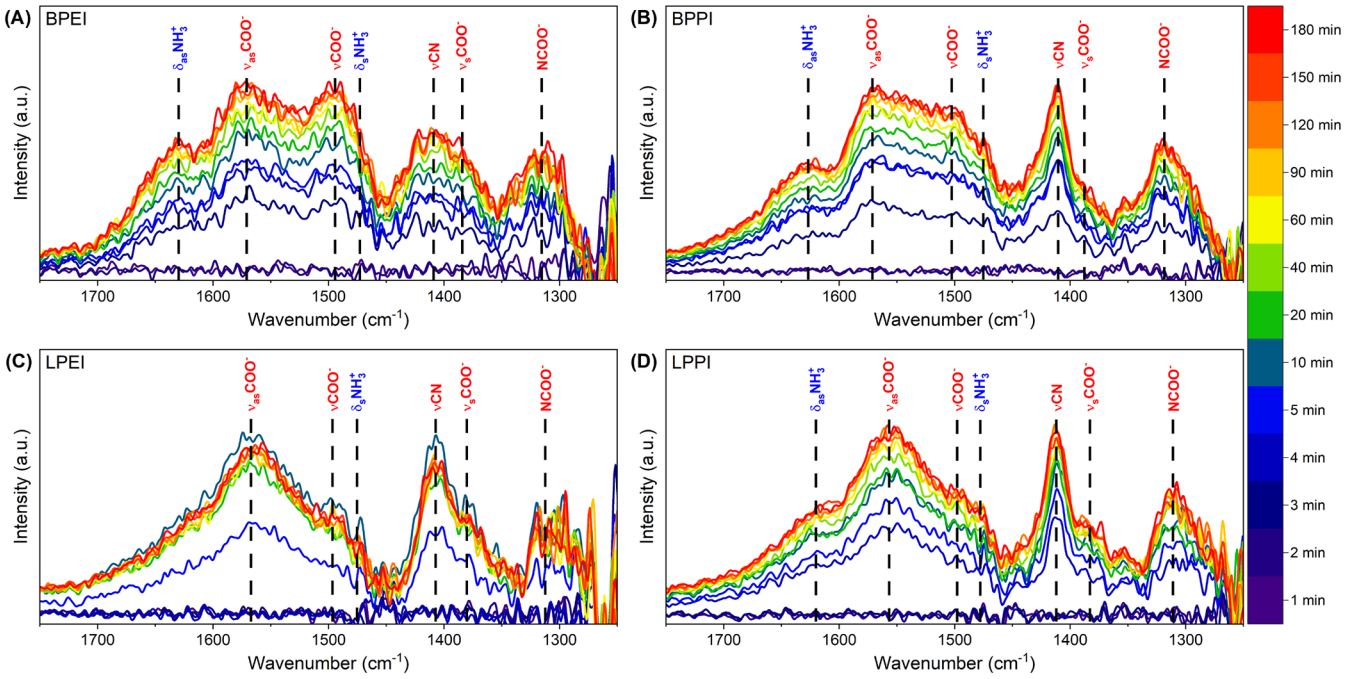

Figure 3. *In situ* FT-IR spectra of (A) BPEI- (B) BPPI- (C) LPEI- and (D) LPPI-impregnated SBA-15 in the presence of flowing 400 ppm of CO_2 at 30 °C.

Table 2. *In Situ* IR Peak Assignments from Reaction of Aminopolymer/SBA-15 Composites in the Presence of 400 ppm of CO_2

Wavenumber [cm^{-1}]	Peak assignment	Group	Reference
1620–1630	$\delta_{as}NH_3^+$	Ammonium ion	56–61
1550–1575	$\nu_{as}COO^-$	Carbamate ion	53,61
1487–1512	νCOO^-	Carbamate ion	56,59,61,62
1475–1486	$\delta_sNH_3^+$	Ammonium ion	53
1410–1420	$\nu CN/NCOO^-$ skeletal vibration	Carbamate ion	54,58,61
1385–1390	ν_sCOO^-	Carbamate ion	53,56,60,63
1300–1325	$NCOO^-$ skeletal vibration	Carbamate ion	54,55,57–59,61

only one smooth peak, suggest that CO_2 is only or primarily adsorbed as ammonium carbamate and that differences in desorption energy result primarily from the respective kinetic/diffusive limitations of each material.

CO_2 Isobars. CO_2 isobars were obtained at constant concentrations of 400 ppm and 10% CO_2 in nitrogen (Figure 4). In each of these experiments, the CO_2 concentration was held constant while the temperature was changed by increments of 10 °C and held for 390 min. Exploring the adsorption performance over a wide range of temperatures enables an initial assessment regarding the type of climate zone in which a particular sorbent material might function well.[64−67] In these experiments, the temperature was first increased to 90 °C (filled points in the figure) then decreased back to 30 °C (hollow points). It has been previously suggested that the shape of the resulting curves indicate the extent to which CO_2 capture at a particular concentration is limited kinetically by pore packing and chain mobility.[33] Earlier work showed that at a concentration of 10% CO_2, the capacity of 1000 g/mol LPPI in SBA-15 first increased with increasing temperature up to 55 °C, after which it decreased during ramping up to 95 °C.[33] Here, we replicated this experiment under 10% CO_2 and also show the behavior under 400 ppm of CO_2. Both the medium and highest amine loadings were tested to ascertain the impact that pore crowding may have. To compare the results across the different sample types, the data in Figure 4 are presented as ΔAE as a function of temperature, where

$$\Delta AE(T) = \frac{AE(T) - AE(30\,^\circ C)}{AE(30\,^\circ C)} \times 100 \quad (1)$$

and AE(T) is the amine efficiency at each temperature, with AE(30 °C) the amine efficiency at 30 °C.

As can be seen at the medium polymer loading and under 400 ppm of CO_2 (Figure 4A), all samples only experience a decrease in capacity with an increase in temperature. This suggests that regardless of the polymer architecture, the adsorption thermodynamics are the limiting factor, as opposed to the CO_2 diffusion rate, such that increased amine mobility has no effect on CO_2 adsorption under DAC conditions. In the high amine loading scenario at 400 ppm (Figure 4C), only the BPEI sample displays a slight enhancement with the increase in temperature, peaking at 50 °C with a 16% improvement before decreasing. Since the corresponding LPPI and BPPI sorbents had similar and even higher levels of pore filling and displayed no improvement with the temperature increase, this result indicates that BPEI has superior mobility within the pores among the polymers studied here.

Under 10% CO_2, the picture is quite different. At this concentration the rate of adsorption begins to outpace the rate of CO_2 diffusion such that diffusive limitations become a contributing factor. At the highest loadings, all materials see a jump in uptake at higher temperatures (Figure 4D). Branched PEI improves the most during heating (+69%) and peaks at the highest temperature across all experiments (80 °C), while

https://doi.org/10.1021/acsapm.5c03465
ACS Appl. Polym. Mater. 2025, 7, 15671−15681

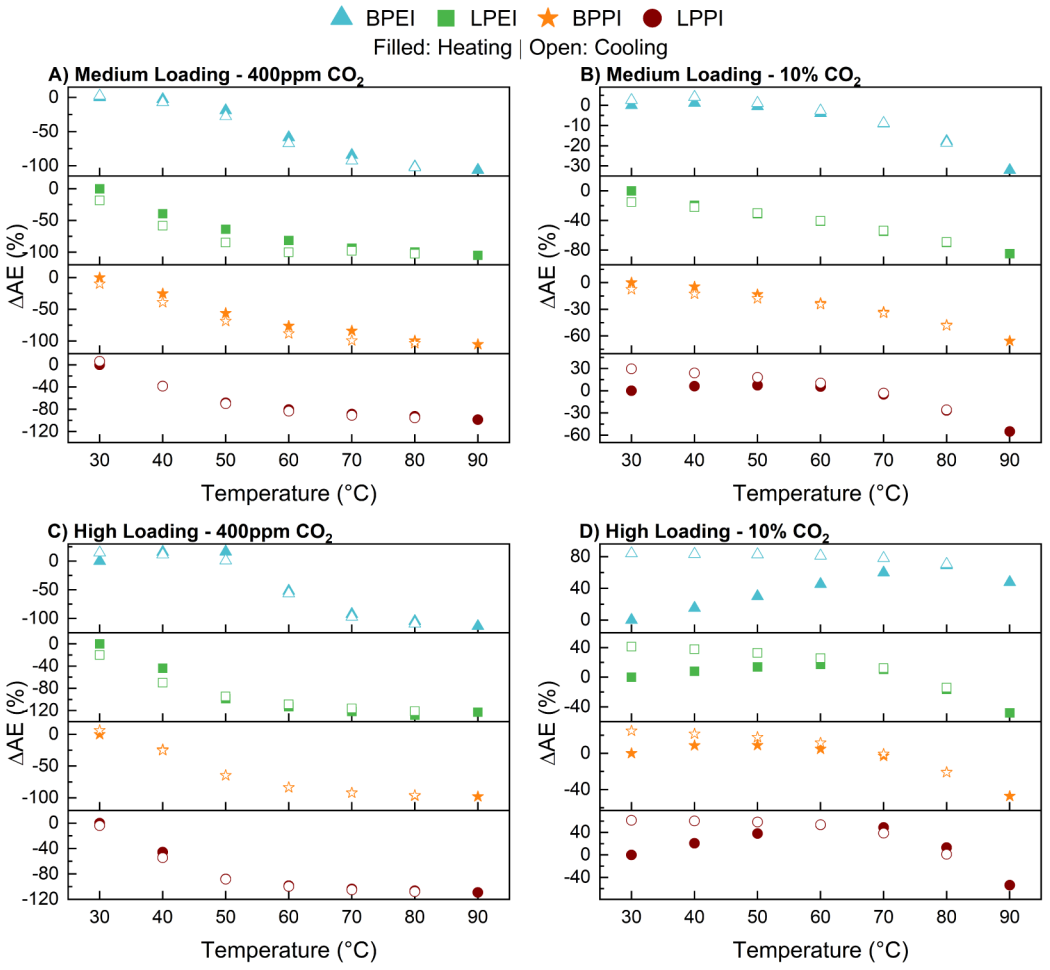

Figure 4. Change in amine efficiency with a change in adsorption temperature under a constant stream of CO_2. ΔAE represents the percent change in amine efficiency compared to its value at 30 °C. The rows (A,B and C,D) represent the medium and high amine loading levels, respectively. The columns (A,C and B,D) represent CO_2 concentrations of 400 ppm and 10%, respectively. Closed and open symbols represent data collected while ramping up and ramping down, respectively, during these isobar measurements.

BPPI improves the least (+9%) and peaks at only 50 °C. The opposite trend is true of the linear species. Though both linear polymers peak at 60 °C during heating, LPPI sees a 53% increase while LPEI only achieves a 17% increase. Interestingly, and as shown previously by Pang et al., all samples see a steady increase in capacity upon cooling, displaying maximums at 30 °C.[33] It was formerly suggested that this is due to the opportunity for CO_2 to penetrate bulk polymer layers at elevated temperatures due to higher CO_2 diffusivity and increased polymer mobility, reacting with amine sites that were previously inaccessible at lower temperatures.

At the medium loading and under 10% CO_2, only BPEI and LPPI display capacity increases with heating, though to a lesser extent than at the high loading (Figure 4B). The capacities of linear PEI and branched PPI only decrease with heating under these conditions. The difference seen across these two loading levels can be attributed to the pore packing. At the highest loading, the pores of the composites, with the exception of LPEI, are close to being completely filled. In this case, as has been previously identified for BPEI/SBA-15 systems, the walls of the pores are completely covered and plug-like aggregates of polymer form, choking axial diffusion of CO_2 deeper into the pores.[68] Therefore, these composites would benefit the most from the diffusive benefits brought about at higher temperatures.

It can also be the case that the significantly different trends at the two CO_2 concentrations are due to the degree of polymer chain cross-linking during the capture process.[69,70] Two amine sites are required for ammonium carbamate formation and whether done inter- or intramolecularly, these pairs form a cross-link that increases the rigidity of the polymer. Since sorption capacity is dependent on the partial pressure of CO_2, at 10% there is greater formation of ammonium carbamate pairs and a higher extent of cross-linking. Thus, a temperature increase is even more important to overcome this more significant barrier at 10% CO_2 conditions, beyond the intrinsic barrier of polymer agglomeration.

CO_2 Sorption/Desorption Cycling. To explore the long-term stability implications of the four different composite types, 25 temperature-swing adsorption−desorption cycles were performed (Figure 5). Following a 3-h initial activation at 110 °C under nitrogen, adsorption occurred at 30 °C for 1 h under 400 ppm of CO_2, followed by a 10 min desorption step at 110 °C in N_2. Figure 5A and C show the amine efficiency at the end of each adsorption step as a function of the cycle number. All four aminopolymers at both loadings demonstrate

https://doi.org/10.1021/acsapm.5c03465
ACS Appl. Polym. Mater. 2025, 7, 15671−15681

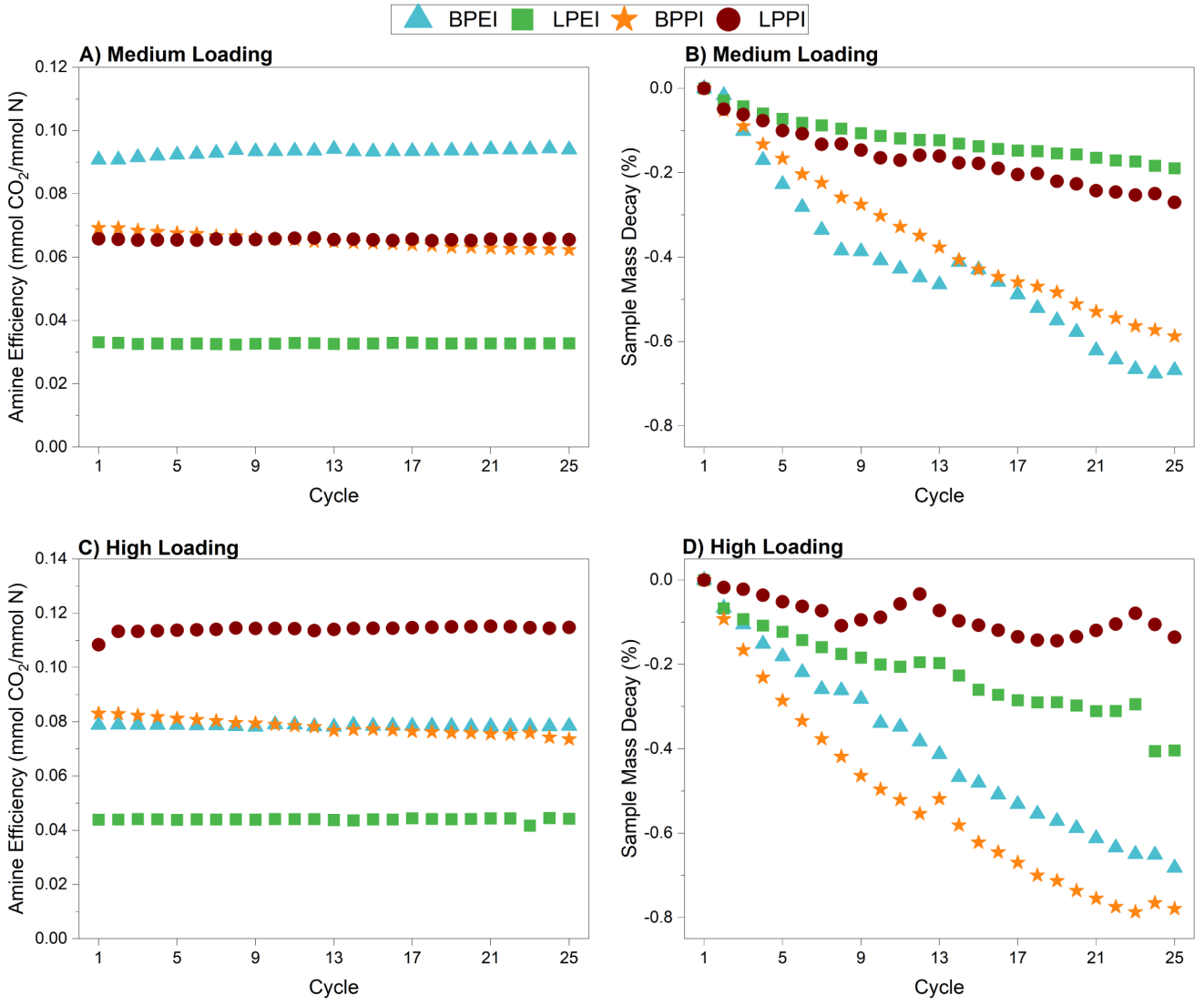

Figure 5. CO_2 adsorption−desorption performance over 25 cycles with temperature swing regeneration. A&C) Amine efficiency as a function of adsorption cycle. Mass change during adsorption was determined using the mass at the beginning of each cycle. B&D) Change in starting sample mass as a function of adsorption cycle. Adsorption performed at 30 °C under 400 ppm of CO_2 for 1 h. Desorption performed under N_2 at 110 °C for 10 min.

decent stability over the TSA cycles. Only BPPI experiences a noteworthy decline in amine efficiency between the first and 25th cycles, by 10% and 11% for the medium and high loading, respectively. Figure 5B and D show the changes in the sample mass at the beginning of each adsorption stage over the course of the experiment. Overall, the decay seen is minimal, with a maximum change of about −0.8% for the high loading BPPI-impregnated SBA-15. At both the high and medium loadings, the linear polymers retain their mass more effectively than the branched polymers. Sample mass decay, particularly to the low degree seen with the linear polymers, could be due to the presence of tough-to-remove water that eventually escapes over repeated dry gas thermal cycling, with the initial 3-h activation period provided at the beginning of the experiment insufficient to remove all water in the first step. As has been previously observed, BPEI is more hydrophilic than LPEI, adsorbing up to 32% more water, which is partly attributed to the different bulk phase of BPEI (viscous liquid) and LPEI (solid).[38] Additionally, the cyclic mass loss could also be due to the presence of low molecular weight oligomeric amines in the branched polymer composites that volatilize during the high temperature desorption period. This could then explain why BPPI suffers from a slight decline in amine efficiency during cycling. Polydisperse, oligomeric amines inherently contain a higher fraction of primary amines than polyamines with a higher degree of polymerization. These primary amines can play an outsized role at low CO_2 concentrations and particularly with a short adsorption period of only 1 h.

CONCLUSIONS

Composite sorbents of PEI and PPI, in both branched and linear architectures, physically impregnated into SBA-15 were tested for their application in direct air capture. Linear and branched PPI as well as linear PEI were synthesized to ensure similar polymer molecular weights across all varieties. The adsorption, desorption and cyclic behavior and performance were investigated under dry conditions. Additionally, a short survey of capacity at elevated temperatures was performed, and *in situ* IR measurements were collected to identify the sorbed species.

https://doi.org/10.1021/acsapm.5c03465
ACS Appl. Polym. Mater. 2025, 7, 15671−15681

The above comparison revealed several insights into how polymer architecture influences CO_2 capture performance under DAC-relevant conditions. LPPI-impregnated SBA-15 sorbents achieved the highest amine efficiency across all loading levels, reaching up to 0.14 mmol CO_2/mmol N, slightly surpassing the BPEI composite. Meanwhile, LPEI exhibited the lowest capacities and amine efficiencies, consistent with previous experimentation, possibly due to its limited polymer mobility and tighter packing within pores. Temperature-programmed desorption studies highlighted that the branched polymers exhibited higher CO_2 desorption energies (102−111 kJ/mol) compared to their linear analogues, suggesting stronger polymer−CO_2 interactions or more effective CO_2 penetration into polymer domains. *In situ* DRIFTS confirmed that all sorbents captured CO_2 primarily as ammonium carbamate. Additionally, isobaric CO_2 uptake tests demonstrated that BPEI maintained better performance under elevated temperatures and concentrations, likely benefiting from enhanced polymer mobility and pore accessibility.

Several limitations exist in extrapolating the results from this model study to practical systems. SBA-15 is not a commercially available support, so future studies should focus on transitioning the aminopolymers into industry-grade alumina or silica often applied in CO_2 capture. Furthermore, though the short-term cyclic studies presented above show no immediate concern of material loss, these materials need to be shown to be resilient across thousands of adsorption/desorption cycles under realistic desorption conditions.[22] Finally, PPI can only be accepted as a possible alternative after its performance is analyzed under more practical conditions, particularly involving humidified gas streams.

■ ASSOCIATED CONTENT

Supporting Information

The Supporting Information is available free of charge at https://pubs.acs.org/doi/10.1021/acsapm.5c03465.

CO_2 isotherms (400 ppm) and uptake data; TPD curves; energy of desorption determination plots; combustion TGA plots; MALDI-TOF results for synthesized branched PPI;^{1}H NMR for synthesized linear PPI and PEI; nitrogen physisorption isotherm for SBA-15; amine-normalized pore fill; XPS; powder XRD of LPPI; monomer and polymer molecular structures (PDF)

■ AUTHOR INFORMATION

Corresponding Author

Christopher W. Jones − *School of Chemical & Biomolecular Engineering, Georgia Institute of Technology, Atlanta, Georgia 30332, United States;* orcid.org/0000-0003-3255-5791; Email: cjones@chbe.gatech.edu

Authors

Jacob Hoffman − *School of Chemical & Biomolecular Engineering, Georgia Institute of Technology, Atlanta, Georgia 30332, United States*

Laura Proaño − *School of Chemical & Biomolecular Engineering, Georgia Institute of Technology, Atlanta, Georgia 30332, United States;* orcid.org/0000-0001-7787-7626

Complete contact information is available at: https://pubs.acs.org/10.1021/acsapm.5c03465

Notes

The authors declare the following competing financial interest(s): C.W.J. has a financial interest in several DAC companies that seek to commercialize CO2 capture from air. C.W.J. has a conflict-of-interest management plan in place at Georgia Tech.

■ ACKNOWLEDGMENTS

This work was supported by the Center for Understanding and Controlling Accelerated and Gradual Evolution of Materials for Energy (UNCAGE-ME), an Energy Frontier Research Center funded by the U.S. Department of Energy, Office of Science, Office of Basic Energy Sciences, under Award No. DE-SC0012577. This work was performed in part at the Georgia Tech Institute for Electronics and Nanotechnology, a member of the National Nanotechnology Coordinated Infrastructure (NNCI), which is supported by the National Science Foundation (ECCS-2025462).

■ REFERENCES

(1) Calvin, K.; Dasgupta, D.; Krinner, G.; Mukherji, A.; Thorne, P. W.; Trisos, C.; Romero, J.; Aldunce, P.; Barrett, K.; Blanco, G., et al. *IPCC, 2023: Climate Change 2023: Synthesis Report. Contribution of Working Groups I, II and III to the Sixth Assessment Report of the Intergovernmental Panel on Climate Change [Core Writing Team, Lee, H. and Romero, J. (Eds.)]*; Arias, P.; Bustamante, M.; Elgizouli, I.; Flato, G.; Howden, M.; Méndez-Vallejo, C.; Pereira, J. J.; Pichs-Madruga, R.; Rose, S. K.; Saheb, Y., Eds.; IPCC: Geneva, Switzerland, 2023. DOI: .

(2) Olabi, A. G.; Abdelkareem, M. A. Renewable Energy and Climate Change. *Renewable Sustainable Energy Rev.* **2022**, *158*, 112111.

(3) Sanz-Pérez, E. S.; Murdock, C. R.; Didas, S. A.; Jones, C. W. Direct Capture of CO $_2$ from Ambient Air. *Chem. Rev.* **2016**, *116* (19), 11840−11876.

(4) Shi, X.; Xiao, H.; Azarabadi, H.; Song, J.; Wu, X.; Chen, X.; Lackner, K. S. Sorbents for the Direct Capture of CO $_2$ from Ambient Air. *Angew. Chem., Int. Ed.* **2020**, *59* (18), 6984−7006.

(5) McQueen, N.; Gomes, K. V.; McCormick, C.; Blumanthal, K.; Pisciotta, M.; Wilcox, J. A Review of Direct Air Capture (DAC): Scaling up Commercial Technologies and Innovating for the Future. *Prog. Energy* **2021**, *3*, 032001.

(6) Bui, M.; Adjiman, C. S.; Bardow, A.; Anthony, E. J.; Boston, A.; Brown, S.; Fennell, P. S.; Fuss, S.; Galindo, A.; Hackett, L. A.; Hallett, J. P.; Herzog, H. J.; Jackson, G.; Kemper, J.; Krevor, S.; Maitland, G. C.; Matuszewski, M.; Metcalfe, I. S.; Petit, C.; Puxty, G.; Reimer, J.; Reiner, D. M.; Rubin, E. S.; Scott, S. A.; Shah, N.; Smit, B.; Trusler, J. P. M.; Webley, P.; Wilcox, J.; Mac Dowell, N. Carbon Capture and Storage (CCS): The Way Forward. *Energy Environ. Sci.* **2018**, *11* (5), 1062−1176.

(7) Bollini, P.; Didas, S. A.; Jones, C. W. Amine-Oxide Hybrid Materials for Acid Gas Separations. *J. Mater. Chem.* **2011**, *21* (39), 15100−15120.

(8) Zhu, X.; Xie, W.; Wu, J.; Miao, Y.; Xiang, C.; Chen, C.; Ge, B.; Gan, Z.; Yang, F.; Zhang, M.; O'Hare, D.; Li, J.; Ge, T.; Wang, R. Recent Advances in Direct Air Capture by Adsorption. *Chem. Soc. Rev.* **2022**, *51*, 6574−6651.

(9) Lyu, H.; Li, H.; Hanikel, N.; Wang, K.; Yaghi, O. M. Covalent Organic Frameworks for Carbon Dioxide Capture from Air. *J. Am. Chem. Soc.* **2022**, *144* (28), 12989−12995.

(10) Zhou, Z.; Ma, T.; Zhang, H.; Chheda, S.; Li, H.; Wang, K.; Ehrling, S.; Giovine, R.; Li, C.; Alawadhi, A. H.; Abduljawad, M. M.; Alawad, M. O.; Gagliardi, L.; Sauer, J.; Yaghi, O. M. Carbon Dioxide Capture from Open Air Using Covalent Organic Frameworks. *Nature* **2024**, *635*, 96−101.

(11) Choi, S.; Gray, M. L.; Jones, C. W. Amine-Tethered Solid Adsorbents Coupling High Adsorption Capacity and Regenerability

for CO2 Capture From Ambient Air. *ChemSusChem* **2011**, *4* (5), 628−635.
(12) Bali, S.; Leisen, J.; Foo, G. S.; Sievers, C.; Jones, C. W. Aminosilanes Grafted to Basic Alumina as CO2 Adsorbents-Role of Grafting Conditions on CO2 Adsorption Properties. *ChemSusChem* **2014**, *7* (11), 3145−3156.
(13) Short, G. N.; Burentugs, E.; Proaño, L.; Moon, H. J.; Rim, G.; Nezam, I.; Korde, A.; Nair, S.; Jones, C. W. Single-Walled Zeolitic Nanotubes: Advantaged Supports for Poly(Ethylenimine) in CO_2 Separation from Simulated Air and Flue Gas. *JACS Au* **2023**, *3* (1), 62−69.
(14) Darunte, L. A.; Oetomo, A. D.; Walton, K. S.; Sholl, D. S.; Jones, C. W. Direct Air Capture of CO2 Using Amine Functionalized MIL-101(Cr). *ACS Sustainable Chem. Eng.* **2016**, *4* (10), 5761−5768.
(15) Lawson, S.; Griffin, C.; Rapp, K.; Rownaghi, A. A.; Rezaei, F. Amine-Functionalized MIL-101 Monoliths for CO2 Removal from Enclosed Environments. *Energy Fuels* **2019**, *33* (3), 2399−2407.
(16) Xu, X.; Song, C.; Andrésen, J. M.; Miller, B. G.; Scaroni, A. W. Preparation and Characterization of Novel CO2 "Molecular Basket" Adsorbents Based on Polymer-Modified Mesoporous Molecular Sieve MCM-41. *Microporous Mesoporous Mater.* **2003**, *62* (1−2), 29−45.
(17) Heydari-Gorji, A.; Sayari, A. Thermal Oxidative, and CO_2 -Induced Degradation of Supported Polyethylenimine Adsorbents. *Ind. Eng. Chem. Res.* **2012**, *51* (19), 6887−6894.
(18) Hunter-Sellars, E.; Kerr, J. D.; Eshelman, H. V.; Pollard, Z. A.; Varni, A. J.; Sakwa-Novak, M. A.; Marple, M. A. T.; Pang, S. H. Oxidation of Supported Amines for CO2 Direct Air Capture: Assessing Impact on Physical Properties and Mobility via NMR Relaxometry. *Macromol. Chem. Phys.* **2024**, *225* (14), 2400023.
(19) Yan, C.; Sayari, A. Spectroscopic Investigation into the Oxidation of Polyethylenimine for CO2 Capture: Mitigation Strategies and Mechanism. *Chem. Eng. J.* **2024**, *479*, 147498.
(20) Li, S.; Guta, Y.; Calegari Andrade, M. F.; Hunter-Sellars, E.; Maiti, A.; Varni, A. J.; Tang, P.; Sievers, C.; Pang, S. H.; Jones, C. W. Competing Kinetic Consequences of CO_2 on the Oxidative Degradation of Branched Poly(Ethylenimine). *J. Am. Chem. Soc.* **2024**, *146*, 28201−28213.
(21) Carneiro, J. S. A.; Innocenti, G.; Moon, H. J.; Guta, Y.; Proaño, L.; Sievers, C.; Sakwa-Novak, M. A.; Ping, E. W.; Jones, C. W. Insights into the Oxidative Degradation Mechanism of Solid Amine Sorbents for CO_2 Capture from Air: Roles of Atmospheric Water. *Angew. Chem., Int. Ed.* **2023**, *62* (24), No. e202302887.
(22) Holmes, H. E.; Banerjee, S.; Vallace, A.; Lively, R. P.; Jones, C. W.; Realff, M. J. Tuning Sorbent Properties to Reduce the Cost of Direct Air Capture. *Energy Environ. Sci.* **2024**, *17* (13), 4544−4559.
(23) Bollini, P.; Choi, S.; Drese, J. H.; Jones, C. W. Oxidative Degradation of Aminosilica Adsorbents Relevant to Postcombustion CO_2 Capture. *Energy Fuels* **2011**, *25* (5), 2416−2425.
(24) Hiyoshi, N.; Yogo, K.; Yashima, T. Adsorption Characteristics of Carbon Dioxide on Organically Functionalized SBA-15. *Microporous Mesoporous Mater.* **2005**, *84* (1−3), 357−365.
(25) Belmabkhout, Y.; Serna-Guerrero, R.; Sayari, A. Amine-Bearing Mesoporous Silica for CO2 Removal from Dry and Humid Air. *Chem. Eng. Sci.* **2010**, *65* (11), 3695−3698.
(26) Darmayanti, M. G.; Tuck, K. L.; Thang, S. H. Carbon Dioxide Capture by Emerging Innovative Polymers: Status and Perspectives. *Adv. Mater.* **2024**, *36*, 2403324.
(27) Wang, D.; Wang, X.; Song, C. Comparative Study of Molecular Basket Sorbents Consisting of Polyallylamine and Polyethylenimine Functionalized SBA-15 for CO2 Capture from Flue Gas. *ChemPhysChem* **2017**, *18* (22), 3163−3173.
(28) Zerze, H.; Tipirneni, A.; McHugh, A. J. Reusable Poly-(Allylamine)-Based Solid Materials for Carbon Dioxide Capture under Continuous Flow of Ambient Air. *Sep. Sci. Technol.* **2017**, *52* (16), 2513−2522.
(29) Sujan, A. R.; Kumar, D. R.; Sakwa-Novak, M.; Ping, E. W.; Hu, B.; Park, S. J.; Jones, C. W. Poly(Glycidyl Amine)-Loaded SBA-15 Sorbents for CO_2 Capture from Dilute and Ultradilute Gas Mixtures. *ACS Appl. Polym. Mater.* **2019**, *1* (11), 3137−3147.
(30) Chaikittisilp, W.; Khunsupat, R.; Chen, T. T.; Jones, C. W. Poly(Allylamine)-Mesoporous Silica Composite Materials for CO 2 Capture from Simulated Flue Gas or Ambient Air. *Ind. Eng. Chem. Res* **2011**, *50* (24), 14203−14210.
(31) Pang, S. H.; Lee, L.-C.; Sakwa-Novak, M. A.; Lively, R. P.; Jones, C. W. Design of Aminopolymer Structure to Enhance Performance and Stability of CO_2 Sorbents: Poly(Propylenimine) vs Poly(Ethylenimine). *J. Am. Chem. Soc.* **2017**, *139* (10), 3627−3630.
(32) Li, S.; Cerón, M. R.; Eshelman, H. V.; Varni, A. J.; Maiti, A.; Akhade, S.; Pang, S. H. Probing the Kinetic Origin of Varying Oxidative Stability of Ethyl- vs. Propyl-spaced Amines for Direct Air Capture. *ChemSusChem* **2023**, *16*, No. e202201908.
(33) Pang, S. H.; Lively, R. P.; Jones, C. W. Oxidatively-Stable Linear Poly(Propylenimine)-Containing Adsorbents for CO_2 Capture from Ultradilute Streams. *ChemSusChem* **2018**, *11* (15), 2628−2637.
(34) Sarazen, M. L.; Sakwa-Novak, M. A.; Ping, E. W.; Jones, C. W. Effect of Different Acid Initiators on Branched Poly(Propylenimine) Synthesis and CO_2 Sorption Performance. *ACS Sustainable Chem. Eng.* **2019**, *7* (7), 7338−7345.
(35) Sarazen, M. L.; Jones, C. W. Insights into Azetidine Polymerization for the Preparation of Poly(Propylenimine)-Based CO_2 Adsorbents. *Macromolecules* **2017**, *50* (23), 9135−9143.
(36) Hack, J.; Frazzetto, S.; Evers, L.; Maeda, N.; Meier, D. M. Branched versus Linear Structure: Lowering the CO2 Desorption Temperature of Polyethylenimine-Functionalized Silica Adsorbents. *Energies* **2022**, *15* (3), 1075.
(37) Zhang, H.; Goeppert, A.; Prakash, G. K. S.; Olah, G. Applicability of Linear Polyethylenimine Supported on Nano-Silica for the Adsorption of CO_2 from Various Sources Including Dry Air. *RSC Adv.* **2015**, *5* (65), 52550−52562.
(38) Zhang, H.; Goeppert, A.; Olah, G. A.; Prakash, G. K. S. Remarkable Effect of Moisture on the CO 2 Adsorption of Nano-Silica Supported Linear and Branched Polyethylenimine. *J. CO2 Util.* **2017**, *19*, 91−99.
(39) Varni, A. J.; Thigpen, L. S.; Calegari Andrade, M. F.; Marple, M. A. T.; Hunter-Sellars, E.; Maiti, A.; Li, S.; Pang, S. H. Understanding the Role of Hydroxyl Functionalization in Linear Poly(Ethylenimine) for Oxidation-Resistant Direct Air Capture of CO_2. *Adv. Sustain. Syst.* **2025**, *9*, 2400960.
(40) Brissault, B.; Kichler, A.; Guis, C.; Leborgne, C.; Danos, O.; Cheradame, H. Synthesis of Linear Polyethylenimine Derivatives for DNA Transfection. *Bioconjugate Chem.* **2003**, *14* (3), 581−587.
(41) Chatani, Y.; Tadokoro, H.; Saegusa, T.; Ikeda, H. Structural Studies of Poly(Ethylenimine). 1. Structures of Two Hydrates of Poly(Ethylenimine): Sesquihydrate and Dihydrate. *Macromolecules* **1981**, *14* (2), 315−321.
(42) Chatani, Y.; Kobatake, T.; Tadokoro, H.; Tanaka, R. Structural Studies of Poly(Ethylenimine). 2. Double-Stranded Helical Chains in the Anhydrate. *Macromolecules* **1982**, *15* (1), 170−176.
(43) Chatani, Y.; Kobatake, T.; Tadokoro, H. Structural Studies of Poly(Ethylenimine). 3. Structural Characterization of Anhydrous and Hydrous States and Crystal Structure of the Hemihydrate. *Macromolecules* **1983**, *16* (2), 199−204.
(44) Li, K.; Jiang, J.; Yan, F.; Tian, S.; Chen, X. The Influence of Polyethyleneimine Type and Molecular Weight on the CO2 Capture Performance of PEI-Nano Silica Adsorbents. *Appl. Energy* **2014**, *136*, 750−755.
(45) Robertson, M.; Qian, J.; Qiang, Z. Polymer Sorbent Design for the Direct Air Capture of CO2. *ACS Appl. Polym. Mater.* **2024**, *6*, 14169−14189.
(46) Didas, S. A.; Kulkarni, A. R.; Sholl, D. S.; Jones, C. W. Role of Amine Structure on Carbon Dioxide Adsorption from Ultradilute Gas Streams Such as Ambient Air. *ChemSusChem* **2012**, *5* (10), 2058−2064.
(47) Borkovec, M.; Koper, G. J. M. Ising Models of Polyprotic Acids and Bases. *J. Phys. Chem.* **1994**, *98* (23), 6038−6045.
(48) Rim, G.; Kong, F.; Song, M.; Rosu, C.; Priyadarshini, P.; Lively, R. P.; Jones, C. W. Sub-Ambient Temperature Direct Air Capture of

CO $_2$ Using Amine-Impregnated MIL-101(Cr) Enables Ambient Temperature CO $_2$ Recovery. *JACS Au* **2022**, *2* (2), 380−393.
(49) Rim, G.; Priyadarshini, P.; Song, M.; Wang, Y.; Bai, A.; Realff, M. J.; Lively, R. P.; Jones, C. W. Support Pore Structure and Composition Strongly Influence the Direct Air Capture of CO $_2$ on Supported Amines. *J. Am. Chem. Soc.* **2023**, *145* (13), 7190−7204.
(50) Al-Marri, M. J.; Kuti, Y. O.; Khraisheh, M.; Kumar, A.; Khader, M. M. Kinetics of CO $_2$ Adsorption/Desorption of Polyethyleneimine-Mesoporous Silica. *Chem. Eng. Technol.* **2017**, *40* (10), 1802−1809.
(51) Song, M.; Rim, G.; Mirzazadeh, G.; Hoffman, J.; Moon, H. J.; Leisen, J. E.; Nik, O. G.; Lively, R. P.; Jones, C. W. Amine-Dependent CO $_2$ Sorption on Amine-Impregnated Mg_2 (dobpdc) MOF under Humid Conditions. *Ind. Chem. Mater.* **2025**, DOI: 10.1039/D5IM00002E.
(52) Cvetanović, R. J.; Amenomiya, Y. Application of a Temperature-Programmed Desorption Technique to Catalyst Studies. *Adv. Catal.* **1967**, *17*, 103−149.
(53) Foo, G. S.; Lee, J. J.; Chen, C.-H.; Hayes, S. E.; Sievers, C.; Jones, C. W. Elucidation of Surface Species through in Situ FTIR Spectroscopy of Carbon Dioxide Adsorption on Amine-Grafted SBA-15. *ChemSusChem* **2017**, *10* (1), 266−276.
(54) Srikanth, C. S.; Chuang, S. S. C. Infrared Study of Strongly and Weakly Adsorbed CO2 on Fresh and Oxidatively Degraded Amine Sorbents. *J. Phys. Chem. C* **2013**, *117* (18), 9196−9205.
(55) Didas, S. A.; Sakwa-Novak, M. A.; Foo, G. S.; Sievers, C.; Jones, C. W. Effect of Amine Surface Coverage on the Co-Adsorption of CO $_2$ and Water: Spectral Deconvolution of Adsorbed Species. *J. Phys. Chem. Lett.* **2014**, *5* (23), 4194−4200.
(56) Danon, A.; Stair, P. C.; Weitz, E. FTIR Study of CO2 Adsorption on Amine-Grafted SBA-15: Elucidation of Adsorbed Species. *J. Phys. Chem. C* **2011**, *115* (23), 11540−11549.
(57) Bacsik, Z.; Atluri, R.; Garcia-Bennett, A. E.; Hedin, N. Temperature-Induced Uptake of CO2 and Formation of Carbamates in Mesocaged Silica Modified with n-Propylamines. *Langmuir* **2010**, *26* (12), 10013−10024.
(58) Wang, X.; Schwartz, V.; Clark, J. C.; Ma, X.; Overbury, S. H.; Xu, X.; Song, C. Infrared Study of CO 2 Sorption over "Molecular Basket" Sorbent Consisting of Polyethylenimine-Modified Mesoporous Molecular Sieve. *J. Phys. Chem. C* **2009**, *113* (17), 7260−7268.
(59) Yu, J.; Chuang, S. S. C. The Structure of Adsorbed Species on Immobilized Amines in CO2 Capture: An in Situ IR Study. *Energy Fuels* **2016**, *30* (9), 7579−7587.
(60) Bacsik, Z.; Ahlsten, N.; Ziadi, A.; Zhao, G.; Garcia-Bennett, A. E.; Martín-Matute, B.; Hedin, N. Mechanisms and Kinetics for Sorption of CO 2 on Bicontinuous Mesoporous Silica Modified with N-Propylamine. *Langmuir* **2011**, *27* (17), 11118−11128.
(61) Wilfong, W. C.; Srikanth, C. S.; Chuang, S. S. C. In Situ ATR and DRIFTS Studies of the Nature of Adsorbed CO2 on Tetraethylenepentamine Films. *ACS Appl. Mater. Interfaces* **2014**, *6* (16), 13617−13626.
(62) Tumuluri, U.; Isenberg, M.; Tan, C. S.; Chuang, S. S. C. In Situ Infrared Study of the Effect of Amine Density on the Nature of Adsorbed CO2 on Amine-Functionalized Solid Sorbents. *Langmuir* **2014**, *30* (25), 7405−7413.
(63) Knöfel, C.; Martin, C.; Hornebecq, V.; Llewellyn, P. L. Study of Carbon Dioxide Adsorption on Mesoporous Aminopropylsilane-Functionalized Silica and Titania Combining Microcalorimetry and in Situ Infrared Spectroscopy. *J. Phys. Chem. C* **2009**, *113* (52), 21726−21734.
(64) Song, M.; Rim, G.; Kong, F.; Priyadarshini, P.; Rosu, C.; Lively, R. P.; Jones, C. W. Cold-Temperature Capture of Carbon Dioxide with Water Coproduction from Air Using Commercial Zeolites. *Ind. Eng. Chem. Res.* **2022**, *61* (36), 13624−13634.
(65) Kong, F.; Rim, G.; Song, M.; Rosu, C.; Priyadarshini, P.; Lively, R. P.; Realff, M. J.; Jones, C. W. Research Needs Targeting Direct Air Capture of Carbon Dioxide: Material & Process Performance Characteristics under Realistic Environmental Conditions. *Korean J. Chem. Eng.* **2022**, *39* (1), 1−19.
(66) Wilson, S. M. W. The Potential of Direct Air Capture Using Adsorbents in Cold Climates. *iScience* **2022**, *25* (12), 105564.
(67) Cai, X.; Coletti, M. A.; Sholl, D. S.; Allen-Dumas, M. R. Assessing Impacts of Atmospheric Conditions on Efficiency and Siting of Large-Scale Direct Air Capture Facilities. *JACS Au* **2024**, *4* (5), 1883−1891.
(68) Holewinski, A.; Sakwa-Novak, M. A.; Jones, C. W. Linking CO $_2$ Sorption Performance to Polymer Morphology in Aminopolymer/Silica Composites through Neutron Scattering. *J. Am. Chem. Soc.* **2015**, *137* (36), 11749−11759.
(69) Kim, H. J.; Chaikittisilp, W.; Jang, K. S.; Didas, S. A.; Johnson, J. R.; Koros, W. J.; Nair, S.; Jones, C. W. Aziridine-Functionalized Mesoporous Silica Membranes on Polymeric Hollow Fibers: Synthesis and Single-Component CO2 and N2 Permeation Properties. *Ind. Eng. Chem. Res.* **2015**, *54* (16), 4407−4413.
(70) Kwon, H. T.; Sakwa-Novak, M. A.; Pang, S. H.; Sujan, A. R.; Ping, E. W.; Jones, C. W. Aminopolymer-Impregnated Hierarchical Silica Structures: Unexpected Equivalent CO $_2$ Uptake under Simulated Air Capture and Flue Gas Capture Conditions. *Chem. Mater.* **2019**, *31* (14), 5229−5237.